Journal Name

ARTICLE

Synthesis and Electronic Structure Determination of Uranium(VI) Ligand Radical Complexes

Khrystyna Herasymchuk,[a] Linus Chiang,[a,b] Cassandra E. Hayes,[a,c] Matthew L. Brown,[a] Jeffrey S. Ovens,[a] Brian Patrick,[d] Daniel B. Leznoff*[a] and Tim Storr*[a]

Pentagonal bipyramidal uranyl (UO_2^{2+}) complexes of salen ligands, *N,N'*-bis(3-*tert*-butyl-(5*R*)-salicylidene)-1,2-phenylenediamine, in which R = ^{t}Bu (**1a**), OMe (**1b**), and NMe$_2$ (**1c**), were prepared and the electronic structure of the one-electron oxidized species **[1a-c]$^+$** were investigated in solution. The solid-state structures of **1a** and **1b** were solved by X-ray crystallography, and in the case of **1b** an asymmetric UO_2^{2+} unit was found due to an intermolecular hydrogen bonding interaction. Electrochemical investigation of **1a-c** by cyclic voltammetry showed that each complex exhibited at least one quasi-reversible redox process assigned to the oxidation of the phenolate moieties to phenoxyl radicals. The trend in redox potentials matches the electron-donating ability of the *para*-phenolate substituents. The electron paramagnetic resonance spectra of cations **[1a-c]$^+$** exhibited g_{av} values of 1.997, 1.999, and 1.995, respectively, reflecting the ligand radical character of the oxidized forms, and in addition, spin-orbit coupling to the uranium centre. Chemical oxidation as monitored by ultraviolet-visible-near-infrared (UV-vis-NIR) spectroscopy afforded the one-electron oxidized species. Weak low energy intra-ligand charge transfer (CT) transitions were observed for **[1a-c]$^+$** indicating localization of the ligand radical to form a phenolate / phenoxyl radical species. Further analysis using density functional theory (DFT) calculations predicted a localized phenoxyl radical for **[1a-c]$^+$** with a small but significant contribution of the phenylenediamine unit to the spin density. Time-dependent DFT (TD-DFT) calculations provided further insight into the nature of the low energy transitions, predicting both phenolate to phenoxyl intervalence charge transfer (IVCT) and phenylenediamine to phenoxyl CT character. Overall, **[1a-c]$^+$** are determined to be relatively localized ligand radical complexes, in which localization is enhanced as the electron donating ability of the *para*-phenolate substituents is increased (NMe$_2$ > OMe > ^{t}Bu).

1 Introduction

Uranium is most commonly found as the uranyl ion (UO_2^{2+}; $5f^06d^0$; U^{VI} oxidation state), which is luminescent,[1] and the excited state is highly oxidizing (E° = 2.6 V vs. SHE) leading to interesting photooxidation chemistry.[2] The chemistry of the UO_2^{2+} ion, with an emphasis on structural modification of the uranyl oxo ligands (O=U=O), and ligand coordination in the equatorial plane, has been previously reviewed.[3] The stabilization and reactivity of uranium, in the U^{III}, U^{IV}, U^{V} and U^{VI} oxidation states, has attracted much research interest in recent years.[4]

Interest in the coordination chemistry of uranium is also due to the need for its safe extraction from soil and water, and stabilization of nuclear waste. For example, crown ethers, phosphorus oxides and salen-type ligands (salen = N_2O_2 bis-Schiff-base bis-phenolate ligands) have been investigated as ligating agents for the extraction of uranium.[5] Uranyl (as well as other *f*-block element) complexes incorporating equatorial Schiff base ligands have been recently studied, as these modular ligands provide a good match in terms of steric and electronic stability.[1,4c,5-6] The first uranyl salophen (phenylenediamine backbone) solid-state structure was reported in 2007, where a coordinating solvent molecule (DMF or DMSO) occupies the fifth equatorial position to afford an overall 7-coordinate complex.[7] It was further shown that in the presence of a noncoordinating solvent, the uranyl salophen complex exists in dimeric form. Uranyl salophen complexes have since been used in several applications including ion recognition of quaternary ammonium and iminium salts, fluoride, dihydrogen phosphate, chloride, formate and acetate.[8] Mazzanti and co-workers have pioneered the

a. *Department of Chemistry, Simon Fraser University, Burnaby, BC, V5A 1S6, Canada Emails: dleznoff@sfu.ca; tim_storr@sfu.ca;*
b. *Current address: Department of Chemistry, Stanford University, Stanford, California 94305, USA*
c. *Current address: Department of Chemistry, University of Rochester, Rochester, New York, 14627, USA*
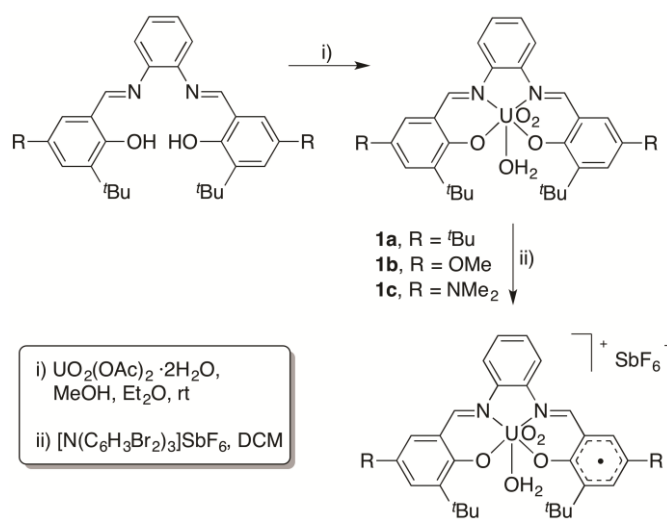d. *Department of Chemistry, University of British Columbia, Vancouver, BC, V6T 1Z1, Canada*

development of magnetic materials containing pentavalent uranyl salophen complexes.[9] In the area of catalysis, the Michael-type addition of thiols and α,β-unsaturated ketones and selected Diels-Alder reactions are catalyzed by uranyl salophen compounds.[10]

In many cases, metal-mediated activation reactions require redox processes to occur at the metal centre, unless redox-active ligands are incorporated into the complex.[11] The use of redox-active ligands in combination with the uranium metal centre has shown significant promise in the field of redox transformations.[12] Bart and co-workers have recently investigated the reduction of uranium complexes containing redox-active ligands.[12d,13] Specifically, reduced U^{III} and U^{IV} complexes, whose oxidation states are stabilized by the redox-active ligands,[14] have been shown to undergo both reductive elimination[15] and oxidative addition,[15b,16] as well as C-F bond activation, showcasing the importance of the ligand system in supporting the uranium oxidation state.[17]

Our group, as well as others, have extensively studied the ligand radical chemistry of tetradentate salens.[18] As an example, salophen metal complexes of Ni,[18d,18o,19] and Cu[18j] have been demonstrated to form ligand radicals upon oxidation. In this work, we report the synthesis and characterization of three neutral uranyl salophen complexes (**1a-c**, see **Scheme 1**, i) incorporating ^tBu, OMe and NMe_2 as *para*-ring substituents. Salophen metal complexes employing ^tBu,[18o,20] OMe[19-20,21] and NMe_2[19] *para*-ring substituents have been previously reported. A recent study[22] reported a U^{VI} tetrathiafulvalene-fused salophen complex with preliminary data on the one-electron oxidized form. An additional study reported the detailed spectroelectrochemical characterization of a singly reduced U(VI) salen ligand radical complex.[6d] Herein, we report the oxidation chemistry of **1a-c** (**Scheme 1**, ii), and analysis of the electronic structure and stability of the one-electron oxidized forms (**[1a-c]$^+$**).

i) $UO_2(OAc)_2 \cdot 2H_2O$, MeOH, Et_2O, rt

ii) $[N(C_6H_3Br_2)_3]SbF_6$, DCM

1a, R = ^tBu
1b, R = OMe
1c, R = NMe_2

Scheme 1. Synthesis of neutral and oxidized $UO_2(Salophen)^R(H_2O)$ complexes; R= ^tBu (**1a**), OMe (**1b**), NMe_2 (**1c**).

2 Experimental

2.1 Materials and Methods

All chemicals used were of the highest grade available and were further purified whenever necessary. The synthesis of the ligand precursors (*N,N'*-bis(3-*tert*-butyl-(5*R*)-salicylidene)-1,2-phenylenediamine, $H_2(Salophen)^R$, in which R = ^tBu, OMe, or NMe_2) has been previously reported.[19] The tris(2,4-dibromophenyl)aminium hexafluoroantimonate radical chemical oxidant, $[N(C_6H_3Br_2)_3]SbF_6$ ($E_{1/2}$ = 1.14 V, MeCN)[23] was synthesized according to published protocols.[24] Acetylferrocenium hexafluoroantimonate, $[AcFc][SbF_6]$ ($E_{1/2}$ = 0.27 V, CH_2Cl_2)[23a] was synthesized following a previously reported method.[25] Electronic spectra were obtained on a Cary 5000 spectrophotometer with a custom-designed immersion fiber-optic probe with a path-length of 10 mm (Hellma, Inc.). Cyclic voltammetry (CV) was performed using a PAR-263A potentiometer, equipped with an Ag wire reference electrode, a glassy carbon working electrode and a Pt counter electrode with $^nBu_4NClO_4$ (0.1 M) solutions in CH_2Cl_2 under an inert atmosphere. Decamethylferrocene was used as an internal standard.[26] Differential pulse voltammetry (DPV) was performed on a CH Instruments 832 Electrochemical Detector, equipped with an Ag wire reference electrode, a Pt disk working electrode and a Pt counter electrode with $^nBu_4NClO_4$ (0.1 M) solutions in CH_2Cl_2. ^1H and ^{13}C NMR spectra were recorded on a Bruker AV-400 instrument. Mass spectra were obtained on Bruker Microflex LT MALDI-TOF MS instrument. Elemental analyses (C, H, N) were performed by Mr. Paul Mulyk at Simon Fraser University on a Carlo Erba EA1110 CHN elemental analyzer. All EPR spectra were collected using a Bruker EMXplus spectrometer operating with a premiumX X-band (~9.5 GHz) microwave bridge. Low temperature measurements (20 K) of frozen solutions used a Bruker helium temperature-control system and a continuous flow cryostat. Samples for X-band measurements were placed in 4 mm outer-diameter sample tubes with sample volumes of ~300 μL. Samples were prepared in capillaries for EPR measurement at 298 K.

2.2 Oxidation protocol

Samples of **[1a-c]$^+$** were prepared at 298 K under nitrogen atmosphere through the addition of a saturated solution of $[N(C_6H_3Br_2)_3]SbF_6$ in CH_2Cl_2 in 50 μL additions to 1.0 mM solutions of **1a-c** in CH_2Cl_2.

2.3 EPR sample preparation

Samples for EPR spectroscopy were prepared by taking an aliquot out of the immersion fiber-optic probe after 1 equivalent of $[N(C_6H_3Br_2)_3]SbF_6$ was added to the **1a-c** solution in CH_2Cl_2 under inert atmosphere (see Section 2.2) and transferred into an EPR tube. EPR tubes containing the **[1a-c]$^+$** solutions were frozen at 77 K and stored until measurement.

2.4 X-ray analysis

Single crystal X-ray crystallographic analysis of **1a** and **1b** was performed on a Bruker SMART diffractometer equipped with an APEX II CCD detector and IμSCuKα (λ = 1.54184 nm) microfocus sealed X-ray tube fitted with HELIOS multilayer optics. Dark red block (**1a** and **1b**) crystals were mounted on MiTeGen dual-thickness MicroMounts using parabar oil. The data was collected at room temperature (approximated to 296 K) (**1a**) and 150(2) K (via an Oxford Cryosystems cold-stream) (**1b**) to a maximum 2θ value of 134˚. Data was collected in a series of φ and ω scans with 1.00˚ image widths and 2 or 5 second exposures. The crystal-to-detector distance was 40 mm. Data was processed using the Bruker APEX II software suite. Using a combination of ShelXle[27] and Olex2[28], the structure was solved with the XT[29] structure solution program using Direct Methods and refined with the ShelXL[30] refinement package using Least Squares minimization. The SQUEEZE algorithm provided by the PLATON (v110516) software package[31] was used to analyze the unmodelled solvent (0.5CH$_3$OH for **1a**), however the final structure was not changed using these programs. All non-hydrogen atoms were refined anisotropically. All C-H hydrogen atoms were placed in geometrically calculated positions without further refinement. OLEX2's *hadd* algorithm was used to geometrically place some water hydrogens. All crystal structure plots were produced using ORTEP-3 and rendered with POV-Ray (v.3.6.2). CCDC numbers 1479739 and 1479740 were obtained for the two structures. A summary of the crystal data and experimental parameters for structure determinations are given in **Table 1.**

2.5 Calculations

Geometry optimization calculations were completed using the Gaussian 09 program (Revision D.01),[32] the B3LYP[33] functional, the 6-31G(d) basis set (C, H, N, O), the SDDAll[34] basis set (U), with a polarized continuum model (PCM) for CH$_2$Cl$_2$ (dielectric ε = 8.94).[35] The use of the SDDAll[34] basis set was based on previously reported theoretical calculations on uranium complexes.[36] Frequency calculations at the same level of theory confirmed that the optimized structures were located at a minimum on the potential energy surface. Single-point calculations and the intensities of 30 lowest energy transitions using TD-DFT[37] calculations were performed using the BHandHLYP[38] functional, the TZVP[39] basis set (C, H, N, O), the SDDAll basis set (U), with a PCM for CH$_2$Cl$_2$.[34]

2.6 Synthesis

2.6.1 Synthesis of UO$_2$(Salophen)^{tBu}(H$_2$O) (1a)

Uranyl acetate dihydrate (0.050 g, 0.12 mmol) was dissolved in methanol (10 mL) and was added to a solution of H$_2$(Salophen)^{tBu} ligand (0.065 g, 0.12 mmol) in methanol (10 mL). The colour of the reaction mixture changed from yellow to red immediately upon the addition of the metal precursor. The reaction solution was stirred for 5 h at room temperature, and the solvent was allowed to evaporate. The crude product was isolated as a brown solid. Recrystallization of **1a** from a concentrated MeOH solution afforded

dark red coloured crystals that were suitable for X-ray diffraction analysis. Yield: (0.097 g, 98%). Elemental analysis (%) calcd for **1a** (C$_{36}$H$_{48}$N$_2$O$_5$U•0.5CH$_3$OH): C, 52.02; H, 5.98; N, 3.32. Found: C, 51.97; H, 5.82; N, 4.09. MALDI-MS *m/z:* 807 ([M-H$_2$O], 100%). IR (ATR): 877 cm^{-1} (v_{as} O=U=O). ^{1}H NMR (400 MHz, CDCl$_3$) δ 9.50 (s, 1H), 7.79 (d, *J* = 2.8 Hz, 1H), 7.58-7.53 (m, 1H), 7.49 (d, *J* = 2.8 Hz, 1H), 7.46-7.41 (m, 1H), 1.73 (s, 9H), 1.35 (s, 9H). ^{13}C NMR (400 MHz, CDCl$_3$) δ 167.9, 166.7, 164.9, 147.1, 137.3, 131.9, 130.3, 128.6, 124.5, 119.9, 35.4, 34.1, 31.7, 30.3.

Table 1. Selected Crystallographic Data for **1a** and **1b**

	1a	1b
Formula	C$_{36}$H$_{48}$N$_2$O$_5$U	C$_{30}$H$_{36}$N$_2$O$_7$U•0.5CHCl$_3$
Formula weight	826.79	834.32
Space group	Pbca	P2$_1$/n
Crystal system	orthorhombic	monoclinic
a (Å)	12.9744(6)	9.4679(4)
b (Å)	17.1766(7)	10.7796(5)
c (Å)	34.6304(13)	30.4674(14)
α (°)	90	90
β (°)	90	91.856(3)
γ (°)	90	90
V [Å^3]	7717.6(6)	3107.9(2)
Z	8	4
T (K)	296(2)	150(2)
ρ_{calcd} (g cm^{-3})	1.451	1.783
λ *(*nm)	1.54184	1.54184
μ (cm^{-1})	12.163	17.208
wR$_2$	0.1896	0.1264
R$_1$	0.0681	0.0559
Goodness-of-fits on F^2	0.993	1.188

2.6.2 Synthesis of UO$_2$(Salophen)^{OMe}(H$_2$O) (1b)

Uranyl acetate dihydrate (0.050 g, 0.12 mmol) was dissolved in methanol (5 mL) and was added to a solution of H$_2$(Salophen)^{OMe} ligand (0.061 g, 0.12 mmol) in diethyl ether (5 mL). The colour of the reaction mixture changed from yellow to red immediately upon the addition of the metal precursor. The reaction solution was stirred for 5 h at room temperature, and the solvent was allowed to evaporate. The crude product was isolated as a dark red/brown solid. Recrystallization of **1b** from a concentrated MeOH solution afforded dark red coloured crystalline solid. Crystals suitable for X-ray diffraction analysis were obtained from slow evaporation of a concentrated CDCl$_3$ solution. Yield: (0.082 g, 85%). Elemental analysis (%) calcd for **1b** (C$_{30}$H$_{36}$N$_2$O$_7$U•2H$_2$O): C, 44.45; H, 4.97; N, 3.46. Found: C, 44.05; H, 4.79; N, 3.06. MALDI-MS *m/z:* 756 ([M-H$_2$O], 100%). IR (ATR): 881 cm^{-1} (v_{as} O=U=O). ^{1}H NMR (400 MHz, acetone-d_6) δ 1.65 (s, 9H), 3.82 (s, 3H), 7.25 (d, *J* = 3.2 Hz, 1H), 7.32 (d, *J* = 3.2 Hz, 1H), 7.50-7.55 (m, 1H), 7.75-7.80 (m, 1H), 9.65 (s, 1H). ^{13}C NMR (400 MHz, acetone-d_6) δ 29.3, 34.9, 55.0, 114.0, 119.9, 123.2, 124.2, 128.5, 141.5, 147.2, 150.6, 165.2, 166.4.

2.6.3 Synthesis of UO$_2$(Salophen)^{NMe2}(H$_2$O) (1c)

Uranyl acetate dihydrate (0.050 g, 0.12 mmol) was dissolved in methanol (5 mL) and was added to a solution of H_2(Salophen)^{NMe2} ligand (0.061 g, 0.12 mmol) in diethyl ether (5 mL). The colour of the reaction mixture changed from yellow to red immediately upon the addition of the metal precursor. The reaction solution was stirred for 5 h at room temperature, and the solvent was allowed to evaporate. The product was isolated as a dark red/brown solid. Yield: (0.068 g, 72%). Elemental analysis (%) calcd for **1c** ($C_{32}H_{42}N_4O_5U$•1CH_3OH•2H_2O): C, 45.62; H, 5.80; N, 6.45. Found: C, 45.46; H, 5.31; N, 5.98. MALDI-MS *m/z:* 781 ([M-H_2O], 100%). IR (ATR): 890 cm^{-1} (v_{as} O=U=O). ^{1}H NMR (400 MHz, acetone-d_6) δ 1.68 (s, 9H), 2.90 (s, 6H), 7.12 (d, *J* = 3.2 Hz, 1H), 7.41 (d, *J* = 3.2 Hz, 1H), 7.48-7.52 (m, 1H), 7.73-7.78 (m, 1H), 9.63 (s, 1H). ^{13}C NMR (400 MHz, acetone-d_6) δ 29.4, 35.1, 41.8, 117.6, 119.8, 123.6, 124.7, 128.2, 140.3, 142.8, 147.2, 166.7.

3 Results and Discussion

3.1 Synthesis and Characterization

The uranium complexes in this study (**1a**-**c**) were synthesized in moderate to good yields by metallation of the salen ligand precursors with $UO_2(OAc)_2$•2H_2O. The diamagnetic complexes (**Scheme 1**) were subsequently characterized by ^{1}H and ^{13}C NMR spectroscopy, elemental analysis, and IR spectroscopy. The data were consistent with expected structures, including binding of an additional water molecule (*vide infra*). Mass spectrometry (MALDI and ESI) was consistent with molecular ions without the additional water molecule. The v_3 asymmetric O=U=O stretch for **1a**-**c** was observed in the IR at 877 cm^{-1}, 881 cm^{-1}, and 890 cm^{-1}, respectively (**Fig. S1**), and are within the range expected for the UO_2^{2+} unit.[40]

3.2 X-ray Crystallography

Crystals suitable for X-ray diffraction analysis of **1a** and **1b** were attained by slow evaporation of concentrated MeOH and $CDCl_3$ solutions of the compounds, respectively and selected crystal data is shown in **Table 1**. The structures of **1a** (**Fig. 1**) and **1b** (**Fig. 2**) are similar and the geometry at uranium in each case is pentagonal bipyramidal including the tetradentate salen ligand, the two oxo ligands, and a water molecule. The tetradentate salen coordination sphere bond distances for **1a** (U-N: 2.491(7) Å and 2.531(7) Å and U-O: 2.249(6) Å and 2.215(6) Å) and **1b** (U-N: 2.529(11) Å and 2.567(11) Å and U-O: 2.206(9) Å and 2.229(8) Å) are consistent with those previously reported for uranyl Schiff base complexes (U-N (2.51-2.65 Å) and U-O (2.20-2.32 Å)).[40a,41] In comparison, the salen coordination sphere bond lengths for the Ni analogue of **1a** are 1.854 Å (Ni-N) and 1.852 Å (Ni-O).[19] The longer coordination sphere bond lengths for **1a** and **1b** lead to significant distortion of the salen ligand in both structures (**Fig. 1** and **2**, insets). The angles between the phenolate planes are 49° (**1a**) and 52° (**1b**), compared to the Ni derivative of 4.5°.[19] Other similar uranyl salen complexes have been reported to exhibit an analogous

curvature of the ligand backbone in order to accommodate the long coordination sphere bond lengths and overall pentagonal bipyramidal structure.[7,40a,41b] Uranyl salen complexes, containing an ethylene backbone,[40a,42] do not exhibit the same ligand distortion, demonstrating that the flexibility of the backbone moiety plays an important role in dictating the degree and type of ligand distortion. The presence of the uranyl unit forces the salen ligand into the equatorial plane, and analysis of the U=O bond lengths for **1a** (1.767(8) Å and 1.787(7) Å) shows that they are essentially identical and within the expected range (1.76-1.79 Å).[40c,41a,43] Interestingly, the uranyl unit is asymmetric in the solid-state structure for **1b** (U=O bond lengths of 1.828(9) Å and 1.750(9) Å). Such asymmetry has been observed previously for uranyl complexes in the solid state[3,44] due to H-bonding,[45] and interactions with Lewis acids,[46] Na$^+$,[40c] and 3d metal ions.[47] The difference of 0.06 Å between the U=O bonds in **1b** is due to an intermolecular H-bond between the O(2) atom and a water molecule in the equatorial plane of an adjacent complex (**Fig. S2**). The water molecule (U-O$_{water}$ 2.575(7) Å (**1a**) and 2.449(10) Å (**1b**)) is weakly coordinated in the fifth equatorial position. Previous findings with similar U^{VI} complexes agree with these observations.[40a,41c,48] It should be noted that MS data for **1a**-**c** shows a molecular ion without the coordinated H_2O molecule. Unfortunately X-ray analysis of **1c** was not possible due to the poor quality of the crystallized material.
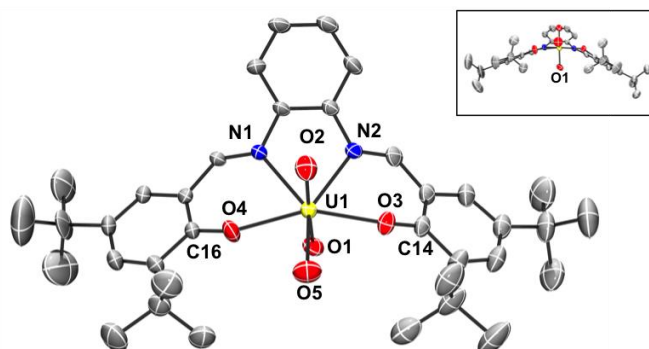
Fig. 1. POV-Ray representation (50% probability) of **1a** excluding hydrogen atoms. Selected interatomic distances [Å]: U(1)-N(1): 2.531(7), U(1)-N(2): 2.491(7), U(1)-O(1): 1.787(7), U(1)-O(2): 1.767(8), U(1)-O(3): 2.215(6), U(1)-O(4): 2.249(6), U(1)-O(5): 2.575(7). Inset: side view of the equatorial plane of the structure showing significant curvature.
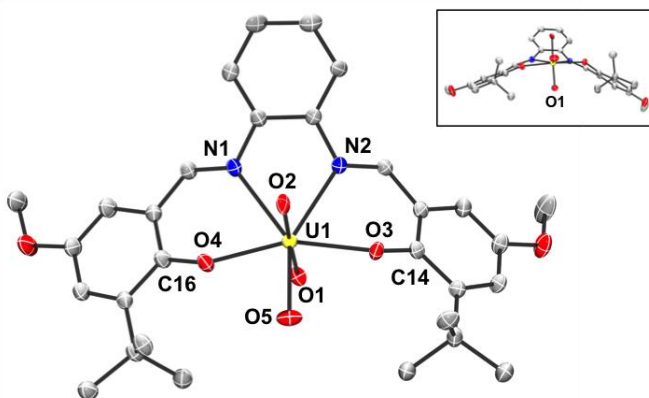

Fig. 2. POV-Ray representation (50% probability) of 1b excluding hydrogen atoms. Selected interatomic distances [Å]: U(1)-N(1): 2.567(11), U(1)-N(2): 2.529(11), U(1)-O(1): 1.750(9), U(1)-O(2): 1.828(9), U(1)-O(3): 2.229(8), U(1)-O(4): 2.206(9), U(1)-O(5):

2.449(10). Inset: side view of the equatorial plane of the structure showing significant curvature.

Table 2. Selected Experimental and Calculated bond lengths (Å) for **1a-c** and **[1a-c]**[+].

	U(1)-N(1)	U(1)-N(2)	U(1)-O(1)	U(1)-O(2)	U(1)-O(3)	U(1)-O(4)	U(1)-O(5)	O(3)-C(14)	O(4)-C(16)
1a[a]	2.531(7)	2.491(7)	1.787(7)	1.767(8)	2.215(6)	2.249(6)	2.575(7)	1.328(10)	1.296(11)
1a[b]	2.543	2.551	1.789	1.793	2.266	2.260	2.599	1.317	1.318
[1a][+b]	2.618	2.519	1.780	1.781	2.214	2.406	2.555	1.323	1.267
1b[a]	2.567(11)	2.529(11)	1.750(9)	1.828(9)	2.229(8)	2.206(9)	2.449(10)	1.327(16)	1.317(16)
1b[b]	2.551	2.559	1.790	1.794	2.260	2.253	2.601	1.322	1.322
[1b][+b]	2.606	2.537	1.781	1.783	2.205	2.404	2.547	1.328	1.271
1c[b]	2.546	2.559	1.792	1.796	2.261	2.252	2.600	1.322	1.323
[1c][+b]	2.596	2.544	1.785	1.786	2.214	2.374	2.565	1.328	1.279

[a] Experimental; [b] Theoretical
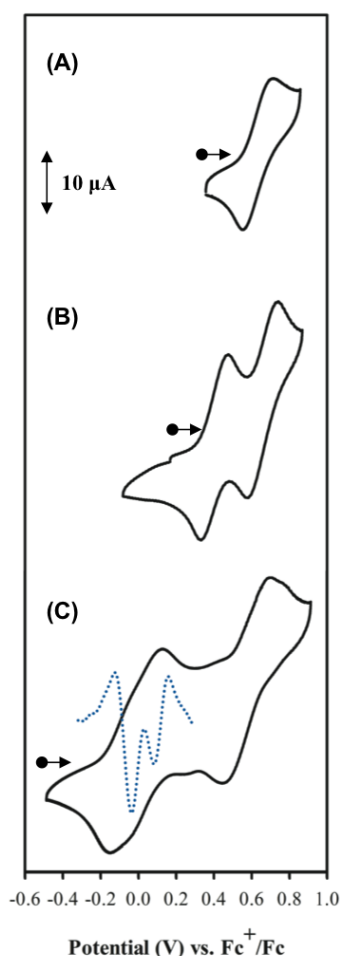
Fig. 3. Cyclic voltammograms of **1a** (A), **1b** (B) and **1c** (C) *versus* Fc[+]/Fc. Conditions: 1.0 mM solutions in CH_2Cl_2, 0.1 M $^nBu_4NClO_4$, T = 298 K. Overlay (blue dotted curve) in (C) shows 2nd derivative of the DPV experiment.

3.3 Electrochemistry

Cyclic voltammetry (CV) was used to probe the redox processes for **1a-c** in CH_2Cl_2 using tetra-*n*-butylammonium perchlorate ($^nBu_4NClO_4$) as the supporting electrolyte (**Fig. 3** and **Table 3**). A previous study on a series of UO_2^{2+} salen complexes reported ligand radical formation from electrochemical analysis.[40a] A quasi-reversible one-electron redox process was observed for **1a** (**Fig. 3A**). Scanning to higher potentials reveals a further irreversible redox process (**Fig. S3A**). Two reversible one-electron redox processes were observed for **1b** (**Fig. 3B**), and scanning to higher potentials reveals a further irreversible redox process (**Fig. S3B**). For **1c**, the increased current intensity and large peak-to-peak difference ($|E_{pa}-E_{pc}|$) in the CV spectrum suggested that the observed spectrum was likely two separate one-electron redox processes (**Fig. 3C**). Differential pulse voltammetry (DPV) was used to determine the redox potentials for the two redox processes at ca. 0 V vs. Fc[+] / Fc (see **Fig. 3C**, inset). The second derivative of the DPV curve affords two peaks with values of -30 mV and 90 mV (See **Fig. S4** for Gaussian fitting and **Fig. S5** for the second derivative curve).

Table 3. Redox potentials for **1a**-**1c** *versus* Fc[+]/Fc[a] (1 mM complex, 0.1 M $^nBu_4NClO_4$, scan rate 100 mV s^{-1}, CH_2Cl_2, 298 K)

UO₂ (Salophen)[R]	$E^1_{1/2}$ (mV)	$E^2_{1/2}$ (mV)	$E^3_{1/2}$ (mV)
R = ^{t}Bu (**1a**)	610 (150)	-	-
R = OMe (**1b**)	400 (110)	660 (120)	-
R = NMe₂ (**1c**)	-30[b]	90[b]	550 (280)

[a] Peak-to-peak differences in brackets ($|E_{pa}-E_{pc}|$ in mV). Peak-to-peak difference for the Fc[+]/Fc couple at 298 K is 200 mV (**1a**); 140 mV (**1b**); 220 mV (**1c**).

[b] Determined by DPV analysis

Due to the electronic structure of the UO_2^{2+} unit (U[VI]; $5f^0 6d^0$), and previous reports on the oxidation of similar metal salen systems,[18a,19,49] the observed redox processes for **1a-c** are assigned to the redox-active phenolate moieties, suggesting ligand-based oxidation processes. The $E_{1/2}$ values for the analogous Ni complexes, employing the same ligands (R= ^{t}Bu, $E_{1/2}$ = 590 mV; R= OMe, $E_{1/2}$ = 360 mV; R= NMe₂, $E_{1/2}$ = -150 mV) match the data in **Table 3** closely.[19] Thus, the decrease in redox potentials of **1a-c**, matching the associated Ni complexes, can be attributed to the increasing donating ability of the *para*-phenolate substituent, and ligand oxidation (*vide infra*). Interestingly, a uranyl complex containing an electron rich cyclo[6]pyrrole ligand has been investigated electrochemically, showcasing ligand-based redox processes at 70 mV and 710 mV vs Fc[+] / Fc.[50] In the following sections we further analyze the one-electron oxidized forms of **1a-c** by electronic spectroscopy, EPR, and theoretical calculations.

3.4 Electronic Spectroscopy

The neutral uranyl salophen complexes **1a-c** exhibit phenolate-uranyl ligand to metal charge transfer (LMCT) bands above 21 000 cm^{-1}, in agreement with previous reports (See **Fig. 4**).[41a,51] Compounds **1a-c** were chemically oxidized using the aminium radical oxidant [N(C$_6$H$_3$Br$_2$)$_3$$^{•}$]$^{+}$ (E$_{1/2}$ = 1.14 V, MeCN)[23a] and the formation of the oxidized species **[1a-c]$^{+}$** were monitored spectrophotometrically (**Fig. 4** and **Table 4**). Broad and weak near-infrared (NIR) bands at 11 000 cm^{-1} for **[1a]$^{+}$** (1500 M^{-1} cm^{-1}) and at 12 500 cm^{-1} for **[1b]$^{+}$** (1000 M^{-1} cm^{-1}) were observed upon oxidation. Oxidation of **1c** (**Fig. 4C**) to **[1c]$^{+}$** was accompanied by the formation of broad higher energy bands in comparison to **[1a-b]$^{+}$** at 17 500 cm^{-1} (7500 M^{-1} cm^{-1}) and 18 500 cm^{-1} (7900 M^{-1} cm^{-1}), and accompanying isosbestic points at 21 500 cm^{-1} and 23 000 cm^{-1}. An identical spectrum for **[1c]$^{+}$** was obtained when using acetylferrocenium (E$_{1/2}$ = 0.27 V, CH$_2$Cl$_2$)[23a] as the chemical oxidant (**Fig. S6**). The stability of **[1a-c]$^{+}$** were monitored over a 5 h period at room temperature. **[1a]$^{+}$** was shown to decay back to neutral **1a** (t$_{1/2}$ = 1 h; **Fig. S7A**). However, both **[1b]$^{+}$** and **[1c]$^{+}$** complexes decay to new species (t$_{1/2}$ = 1.5 h and 1 h, respectively) with three and two isosbestic points observed respectively during decay (**Fig. S7B** and **C**).

Table 4. UV-Vis-NIR Data of **[1a]$^{+}$**, **[1b]$^{+}$** and **[1c]$^{+}$**.

Complex	ν/cm^{-1} (ε/10^3 M^{-1} cm^{-1})
1a	27 500 (15), 23 000 sh (7.5)
[1a]$^{+}$	26 000 (20), 17 000 sh (1.5), 11 000 (1.5)
1b	25 500 (10)
[1b]$^{+}$	26 000 (17.5), 22 000 sh (9), 20 000 sh (6.5), 12500 (1)
1c	28 500 sh (10), 22 500 (6.5)
[1c]$^{+}$	26 500 (15), 18 500 (7.9), 17 500 (7.5)

The broad and weak NIR transitions observed for both **[1a-b]$^{+}$** (ε_{max} ≤ 5000 cm^{-1}; $\Delta\nu_{1/2}$ ≥ 3200 cm^{-1}) are consistent with a localized phenoxyl radical species and a Class II system in the Robin and Day classification system.[52] As a comparison, the oxidized Ni salen complex employing the cyclohexyl backbone [Nisalcn]$^{+}$ exhibits a sharp and intense ligand radical NIR band (ε_{max} = 22000 M^{-1} cm^{-1}) and is characterized as a delocalized Class III system.[18d] Interestingly, the oxidized Ni analogue of **1a** also displays a relatively weak NIR band, but at much lower energy (ε_{max} = 3600 cm^{-1}; $\Delta\nu_{1/2}$ ≥ 3700 cm^{-1}), yet has been characterized as a delocalized radical system.[18o,19] Participation of the *o*-phenylenediamine backbone in the low energy transition increases intra-ligand charge transfer character, adding additional complexity to the band analysis.[18o] The presence of two low energy bands in the spectrum of **[1c]$^{+}$** likely leads to the overall increased intensity for the low energy features associated with this derivative. Theoretical calculations on **[1a-c]$^{+}$** (*vide infra*) provide further information on the electronic structure and nature of the NIR transitions.
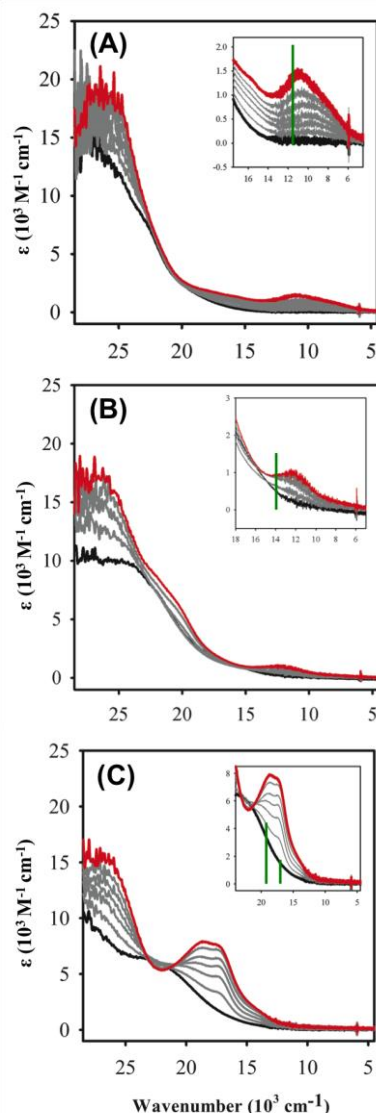

Fig. 4. Electronic spectra of the chemical oxidation of **1a** (black) to **[1a]$^{+}$** (red) in (A), **1b** (black) to **[1b]$^{+}$** (red) in (B) and **1c** (black) to **[1c]$^{+}$** (red) in (C). Oxidation was completed *via* titration (grey lines) with [N(C$_6$H$_3$Br$_2$)$_3$]SbF$_6$. Conditions: 1.0 mM solution in CH$_2$Cl$_2$, T = 298 K. Insets show low energy transitions. Vertical green inset lines are TD-DFT predictions for the low energy transitions.

3.5 Electron paramagnetic resonance

EPR spectroscopy was employed to further characterize the electronic structure of complexes **[1a-c]$^{+}$**. The EPR spectrum of **[1a]$^{+}$** at 20 K (**Fig. 5A**) exhibits a rhombic S = ½ EPR signal at g$_{av}$ = 1.997 (g$_1$ = 2.005, g$_2$ = 1.995, g$_3$ = 1.991), which is slightly lower in comparison to the free electron value (g$_e$ = 2.002).[53] This low g$_{av}$ value for the phenoxyl radical, in comparison to g$_e$, can be rationalized due to interaction of the unpaired spin with the large spin-orbit coupling associated with the uranium nucleus (U^{6+}; 5f^{0}6d^0).[6c,18i] A recent example by Bart *et al.*, reported two uranyl complexes containing redox-active ligands that have g values of 1.974 and 1.936.[12e] In each case, the unpaired spin was assigned to the ligand moiety, with the low g-values due to spin-orbit coupling to the uranium

centre.[12e] The EPR spectrum of **[1b]**[+] at 20 K (**Fig. 5B**) displays a rhombic S = ½ EPR signal at g_{av} = 1.999 (g_1 = 2.004, g_2 = 2.000, g_3 = 1.993), with the low g_{av} value likely due to interaction of the phenoxyl radical with the uranium nucleus as described for **[1a]**[+]. The EPR spectrum of **[1c]**[+] at 20 K (**Fig. 5C**) also shows a rhombic EPR signal (S = ½) at g_{av} = 1.995 (g_1 = 1.997, g_2 = 1.991, g_3 = 1.997), however the signal is much broader in comparison to **[1a]**[+] and **[1b]**[+]. Signal broadness for **[1c]**[+] could be due to unresolved ligand hyperfine interactions.[6c,18a] We next investigated the oxidation of **1a-c** at 298 K with 0.5 equiv. of [N(C$_6$H$_3$Br$_2$)$_3$]SbF$_6$ to ensure complete consumption of the oxidant. The formation of ligand radical species was observed by EPR for all three complexes at 298 K (**Fig. S8**), and additionally hyperfine coupling was observed for **[1a]**[+] (**Fig. S8A**) and **[1c]**[+] (**Fig. S8C**). While sample decomposition occurred over time in the 298 K EPR samples, the hyperfine coupling provides further evidence for localization of the ligand radical for **[1a]**[+] and **[1c]**[+]. A lack of hyperfine coupling for **[1b]**[+] is likely due to line broadening. Overall, the EPR spectra of **[1a-c]**[+] are in agreement with ligand radical formation upon oxidation of **1a-c**.
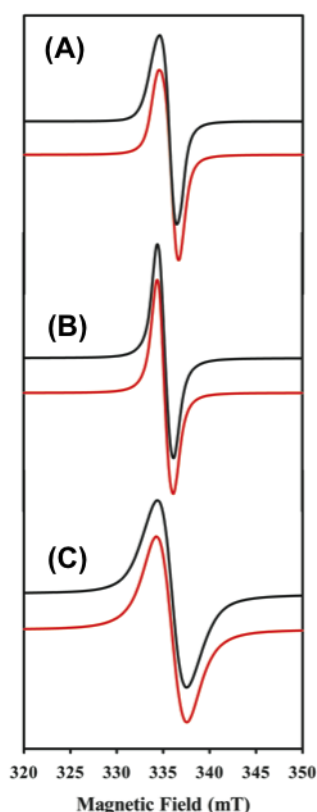

Fig. 5. X-Band EPR spectra for **[1a]**[+] (A), **[1b]**[+] (B), and **[1c]**[+] (C) in CH$_2$Cl$_2$ (black) with respective simulated spectra (red); (A) g_1 = 2.005, g_2 = 1.995, g_3 = 1.991, g_{av} = 1.997; Hstrain: 26.8076; (B) g_1 = 2.004, g_2 = 2.000, g_3 = 1.993, g_{av} = 1.999; Hstrain: 11.8160; (C) g_1 = 1.997, g_2 = 1.991, g_3 = 1.997 g_{av} = 1.995; Hstrain: 62.7626. Conditions: 1.0 mM; frequency, 9.38 GHz; power, 2.00 mW; modulation frequency, 100 kHz; amplitude, 0.6 mT; T = 20 K.

3.6 Theoretical calculations

The geometric and electronic structures of neutral **1a-c** and oxidized **[1a-c]**[+] were further studied using density functional theory (DFT). The calculated metrical data for the coordination sphere bond lengths of **1a-b** agree with the X-ray bond lengths within 0.05 Å (**Table 2**). However, the difference in bond length between experimental and theoretical values of U-O$_{water}$ in **1b** is 0.15 Å due to the participation of the water molecule in H-bonding. Furthermore, the intermolecular H-bonding between O(2) that was observed in solid-state for **1b**, (*vide supra*) was not observed in the geometry optimized structure, where U=O bond lengths for **1b** were predicted to be 1.7896 and 1.7943 Å. A slight asymmetry was predicted for the salen U-O and U-N coordination sphere bond lengths of the oxidized complexes, **[1a-c]**[+] (as seen in **Table 2**), which further supports the phenolate / phenoxyl electronic structure for **[1a-c]**[+]. Moreover, the phenoxyl oxygen-carbon bond lengths in **[1a-c]**[+] (O(3)-C(14)) are significantly shorter in comparison to their phenolate counterparts (O(4)-C(16)) (see **Table 2**). This shortening of the O-C bond on one of the phenolate units, further supports a localized phenoxyl ligand radical formation for all three derivatives.

Spin density (SD) plots of **[1a-c]**[+] show a localized ligand radical for each derivative, as depicted in **Fig. 6**. The data for **[1a]**[+], contrasts with that reported for the Ni analogue,[18o] in which a delocalized ligand radical is predicted and observed experimentally. This difference in electronic structure further illustrates the critical role that the metal ion plays as the bridging component in these ligand radical systems.[18g,18h,54] The high-valent uranyl ion results in minimal electronic coupling between the redox-active phenolates and ligand radical localization, as has been previously observed in Mn and Co systems.[18h,54] Distortion of the salen ligand may also contribute to radical localization. Interestingly, while the majority of the spin density is observed on the phenoxyl moiety for **[1a]**[+] (85%), a significant amount is based on the phenylenediamine backbone (13%). The predicted spin density on the phenoxyl moiety increases for the oxidized OMe derivative **[1b]**[+] (90%), and the NMe$_2$ derivative **[1c]**[+] (96%), with a concomitant decrease in the phenylenediamine spin density (**Fig. 6**). The increased localization of the spin density on the phenoxyl (NMe$_2$ > OMe > ^{t}Bu) showcases the effect the *para*-phenolate substituent on the overall electronic structure.
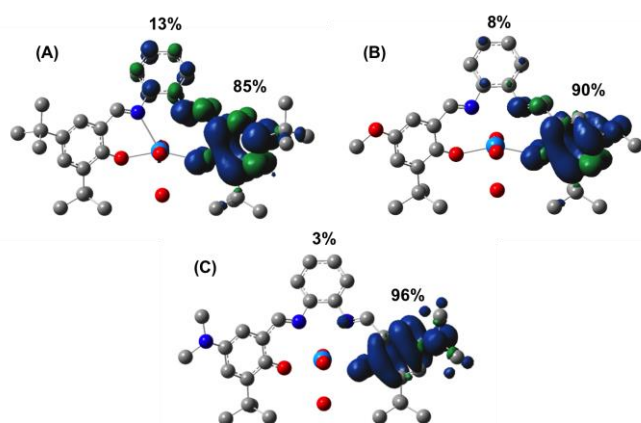
Fig. 6. Predicted spin density of **[1a]$^+$** (A), **[1b]$^+$** (B) and **[1c]$^+$** (C). See Experimental Section for calculation details.

Time-dependent DFT (TD-DFT)[55] calculations were used to gain insight into the low-energy transitions of **[1a-c]$^+$**. The predicted bands for the three oxidized derivatives match the experimental energies as shown in **Fig. 4**, and show a trend in increasing energies as the electron-donating ability of the *para*-phenolate substituent is increased. One low energy band of significant intensity was predicted for each of **[1a]$^+$** and **[1b]$^+$**, while two higher energy transitions were predicted for **[1c]$^+$**. The natural transition orbitals (NTOs)[56] contributing to the transitions are shown in **Table 5**. The low energy band for **[1a]$^+$** is predicted to be a ligand-based charge transfer (CT) transition with the acceptor orbital based primarily on the phenoxyl ring. Interestingly, the donor orbital contains significant phenylenediamine and phenoxyl character, with a smaller contribution from the phenolate. Further analysis of the individual orbital contributions to the low energy band for **[1a]$^+$** shows that the β-HOMO-1 → β-LUMO transition contains significant intervalence charge transfer (IVCT) character as expected for a localized phenoxyl radical electronic structure (**Fig. S9**). The phenylenediamine unit in the delocalized Ni analogue of **[1a]$^+$** is also predicted to contribute to the intraligand CT character of the low energy band,[18o] differing from the results for the saturated cyclohexanediamine backbone.[18d] The predicted donor and acceptor orbitals for the oxidized OMe (**[1b]$^+$**) and NMe$_2$ (**[1c]$^+$**) complexes are qualitatively similar to **[1a]$^+$**, the major difference being the increased IVCT character. This is manifested in the increased phenolate character in the donor orbital, and increased *para*-phenolate substituent character in the acceptor orbital (**Table 5**). This increased IVCT character (^{t}Bu < OMe < NMe$_2$) in the oxidized complexes is likely responsible for the predicted blue-shift in the low energy band, matching the experimental trend. **[1c]$^+$** exhibited an additional band at 18500 cm^{-1}, which is assigned to a transition localized on the phenoxyl unit (**Fig. S9**, **Table 5**). Furthermore, we compared the computational results to **[1a-c]$^+$** without the coordinated water molecule. Interestingly, the spin density (**Fig. S10**) and TD-DFT predictions are essentially the same for **[1a-c]$^+$** with or without

the coordinated water molecule. Thus, based on our current experimental and theoretical results it is unclear if the water molecule remains bound upon oxidation, however, we expect the oxidized complexes to exhibit increased Lewis acidity due to weaker ligation of the phenoxyl moiety.

Table 5. Natural Transition Orbitals (NTOs) representing the dominant low energy transitions of [**1a**]$^+$, [**1b**]$^+$ and [**1c**]$^+$.

	Excited State Properties	Donor	Acceptor
[1a]$^+$	Excited State 1 v_{calc} = 11520 cm^{-1} f = 0.0866 v_{exp} = 11000 cm^{-1} ε = 1500 M^{-1} cm^{-1}		
[1b]$^+$	Excited State 1 v_{calc} = 13927 cm^{-1} f = 0.0544 v_{exp} = 12500 cm^{-1} ε = 1000 M^{-1} cm^{-1}		
[1c]$^+$	Excited State 3 v_{calc} = 16863 cm^{-1} f = 0.0831 v_{exp} = 17500 cm^{-1} ε = 7500 M^{-1} cm^{-1}		
	Excited State 4 v_{calc} = 19231 cm^{-1} f = 0.2310 v_{exp} = 18500 cm^{-1} ε = 7900 M^{-1} cm^{-1}		

4 Summary

In this work a series of uranyl salen complexes **1a-c** have been synthesized with differing *para*-phenolate substituents to probe the effect of ligand electronics on the electronic structure of the oxidized forms **[1a-c]$^+$**. The oxidized complexes are shown to be relatively localized ligand radical complexes, in which localization is enhanced as the electron donating ability of the *para*-phenolate substituents is increased (NMe$_2$ > OMe > ^{t}Bu). The relatively weak and broad low energy ligand CT transitions observed for **[1a-c]$^+$** exhibit both intervalence charge transfer (IVCT) character and an additional contribution from the phenylenediamine backbone, providing further information on the localized ligand radical character of these oxidized uranyl complexes.

5 Acknowledgements

6 References

1. H. Kunkely, Vogler, A., *Z. Naturforsch.*, 2002, **57 b**, 4.

2. (a) X.-S. Zhai, Y.-Q. Zheng, J.-L. Lin and W. Xu, *Inorg. Chim. Acta*, 2014, **423**, 1-10; (b) S. M. Fonseca, H. D. Burrows, M. G. Miguel, M. Sarakha and M. Bolte, *Photochem. Photobiol. Sci.*, 2004, **3**, 317-321; (c) W.-D. Wang, A. Bakac and J. H. Espenson, *Inorg. Chem.*, 1995, **34**, 6034-6039; (d) L. S. Natrajan, *Coord. Chem. Rev.*, 2012, **256**, 1583-1603; (e) A. B. Yusov and V. P. Shilov, *Russ. Chem. B.*, 2000, **49**, 1925-1953; (f) H. D. Burrows and T. J. Kemp, *Chem. Soc. Rev.*, 1974, **3**, 139-165.

3. S. Fortier and T. W. Hayton, *Coord. Chem. Rev.*, 2010, **254**, 197-214.

4. (a) J. D. Van Horn and H. Huang, *Coord. Chem. Rev.*, 2006, **250**, 765-775; (b) Z. Szabó, T. Toraishi, V. Vallet and I. Grenthe, *Coord. Chem. Rev.*, 2006, **250**, 784-815; (c) J. Sessler, P. Melfi and G. Pantos, *Coord. Chem. Rev.*, 2006, **250**, 816-843; (d) P. L. Arnold, J. B. Love and D. Patel, *Coord. Chem. Rev.*, 2009, **253**, 1973-1978; (e) N. H. Anderson, H. Yin, J. J. Kiernicki, P. E. Fanwick, E. J. Schelter and S. C. Bart, *Angew. Chem. Int. Ed.*, 2015, **54**, 9386-9389; (f) E. A. Pedrick, G. Wu, N. Kaltsoyannis and T. W. Hayton, *Chem. Sci.*, 2014, **5**, 3204-3213; (g) P. L. Arnold, S. M. Mansell, L. Maron and D. McKay, *Nat. Chem.*, 2012, **4**, 668-674; (h) S. T. Liddle, *Angew. Chem. Int. Ed.*, 2015, **54**, 8604-8641; (i) A. R. Fox, S. C. Bart, K. Meyer and C. C. Cummins, *Nature*, 2008, **455**, 341-349; (j) D. P. Halter, F. W. Heinemann, J. Bachmann and K. Meyer, *Nature*, 2016, **530**, 317-321; (k) P. L. Arnold, G. M. Jones, S. O. Odoh, G. Schreckenbach, N. Magnani and J. B. Love, *Nat. Chem.*, 2012, **4**, 221-227.

5. Z. Asadi and M. R. Shorkaei, *Spectrochim. Acta Mol. Biomol. Spectrosc.*, 2013, **105**, 344-351.

6. (a) M. S. Bharara, K. Heflin, S. Tonks, K. L. Strawbridge and A. E. Gorden, *Dalton Trans.*, 2008, 2966-2973; (b) D. J. Evans, P. C. Junk and M. K. Smith, *Polyhedron*, 2002, **21**, 2421-2431; (c) N. H. Anderson, S. O. Odoh, U. J. Williams, A. J. Lewis, G. L. Wagner, J. Lezama Pacheco, S. A. Kozimor, L. Gagliardi, E. J. Schelter and S. C. Bart, *J. Am. Chem. Soc.*, 2015, **137**, 4690-4700; (d) K. Takao, S. Tsushima, T. Ogura, T. Tsubomura and Y. Ikeda, *Inorg. Chem.*, 2014, **53**, 5772-5780.

7. K. Takao and Y. Ikeda, *Inorg. Chem.*, 2007, **46**, 1550-1562.

8. (a) M. Cametti, M. Nissinen, A. D. Cort, L. Mandolini and K. Rissanen, *J. Am. Chem. Soc.*, 2007, **129**, 3641-3648; (b) M. Cametti, A. Dalla Cort, L. Mandolini, M. Nissinen and K. Rissanen, *New J. Chem.*, 2008, **32**, 1113; (c) M. Cametti, A. Dalla Cort and K. Bartik, *ChemPhysChem*, 2008, **9**, 2168-2171; (d) D. M. Rudkevich, W. P. R. V. Stauthamer, W. Verboom, J. F. J. Engbersen, S. Harkema and D. N. Reinhoudt, *J. Am. Chem. Soc.*, 1992, **114**, 9671-9673; (e) E. Bodo, A. Ciavardini, A. Dalla Cort, I. Giannicchi, F. Yafteh Mihan, S. Fornarini, S. Vasile, D. Scuderi and S. Piccirillo, *Chem. Eur. J.*, 2014, **20**, 11783-11792; (f) M. Hosseini, M. R. Ganjali, B. Veismohammadi, F. Faridbod, S. D. Abkenar and M. Salavati-Niasari, *Luminescence*, 2012, **27**, 341-345.

9. (a) V. Mougel, L. Chatelain, J. Hermle, R. Caciuffo, E. Colineau, F. Tuna, N. Magnani, A. de Geyer, J. Pecaut and M. Mazzanti, *Angew. Chem. Int. Ed.*, 2014, **53**, 819-823; (b) P. Horeglad, G. Nocton, Y. Filinchuk, J. Pecaut and M. Mazzanti, *Chem. Commun.*, 2009, 1843-1845; (c) V. Mougel, L. Chatelain, J. Pecaut, R. Caciuffo, E. Colineau, J. C. Griveau and M. Mazzanti, *Nat. Chem.*, 2012, **4**, 1011-1017; (d) V. Vetere, P. Maldivi and M. Mazzanti, *C. R. Chim.*, 2010, **13**, 876-883.

10. (a) A. Dalla Cort, L. Mandolini and L. Schiaffino, *Chem. Commun.*, 2005, 3867-3869; (b) V. van Axel Castelli, A. Dalla Cort, L. Mandolini, D. N. Reinhoudt and L. Schiaffino, *Chem. Eur. J.*, 2000, **6**, 1193-1198; (c) V. C. van Axel Castelli, A. D., Mandolini, L., *J. Am. Chem. Soc.*, 1998, **120**, 2; (d) V. van Axel Castelli, F. Bernardi, A. Dalla Cort, L. Mandolini, I. Rossi and L. Schiaffino, *J. Org. Chem.*, 1999, **64**, 8122-8126; (e) A. Dalla Cort, L. Mandolini and L. Schiaffino, *J. Org. Chem.*, 2008, **73**, 9439-9442; (f) V. van Axel Castelli, A. Dalla Cort, L. Mandolini, David N. Reinhoudt and L. Schiaffino, *Eur. J. Org. Chem.*, 2003, **2003**, 627-633.

11. (a) C. T. Lyons and T. D. Stack, *Coord. Chem. Rev.*, 2013, **257**, 528-540; (b) P. J. Chirik and K. Wieghardt, *Science*, 2010, **327**, 794-795; (c) J. W. Whittaker, *Chem. Rev.*, 2003, **103**, 2347-2363; (d) J. Rittle and M. T. Green, *Science*, 2010, **330**, 933-937.

12. (a) E. J. Schelter, R. Wu, J. M. Veauthier, E. D. Bauer, C. H. Booth, R. K. Thomson, C. R. Graves, K. D. John, B. L. Scott, J. D. Thompson, D. E. Morris and J. L. Kiplinger, *Inorg. Chem.*, 2010, **49**, 1995-2007; (b) J. J. Kiernicki, B. S. Newell, E. M. Matson, N. H. Anderson, P. E. Fanwick, M. P. Shores and S. C. Bart, *Inorg. Chem.*, 2014, **53**, 3730-3741; (c) S. J. Kraft, P. E. Fanwick and S. C. Bart, *Inorg. Chem.*, 2010, **49**, 1103-1110; (d) S. A. Pattenaude, C. S. Kuehner, W. L. Dorfner, E. J. Schelter, P. E. Fanwick and S. C. Bart, *Inorg. Chem.*, 2015, **54**, 6520-6527; (e) J. J. Kiernicki, D. P. Cladis, P. E. Fanwick, M. Zeller and S. C. Bart, *J. Am. Chem. Soc.*, 2015, **137**, 11115-11125.

13. N. H. Anderson, S. O. Odoh, Y. Yao, U. J. Williams, B. A. Schaefer, J. J. Kiernicki, A. J. Lewis, M. D. Goshert, P. E. Fanwick, E. J. Schelter, J. R. Walensky, L. Gagliardi and S. C. Bart, *Nat. Chem.*, 2014, **6**, 919-926.

14. (a) N. H. Anderson, S. O. Odoh, Y. Yao, U. J. Williams, B. A. Schaefer, J. J. Kiernicki, A. J. Lewis, M. D. Goshert, P. E. Fanwick, E. J. Schelter, J. R. Walensky, L. Gagliardi and S. C. Bart, *Nat Chem*, 2014, **6**, 919-926; (b) E. M. Matson, J. J. Kiernicki, N. H. Anderson, P. E. Fanwick and S. C. Bart, *Dalton Trans.*, 2014, **43**, 17885-17888.

15. (a) E. M. Matson, S. M. Franke, N. H. Anderson, T. D. Cook, P. E. Fanwick and S. C. Bart, *Organometallics*, 2014, **33**, 1964-1971; (b) E. Lu and S. T. Liddle, *Dalton Trans.*, 2015, **44**, 12924-12941.

16. J. J. Kiernicki, P. E. Fanwick and S. C. Bart, *Chem. Commun.*, 2014, **50**, 8189-8192.

17. (a) J. T. Coutinho, M. A. Antunes, L. C. Pereira, J. Marcalo and M. Almeida, *Chem. Commun.*, 2014, **50**, 10262-10264; (b) C. L. Clark, J. J. Lockhart, P. E. Fanwick and S. C. Bart, *Chem. Commun.*, 2015, **51**, 14084-14087.

18. (a) L. Chiang, A. Kochem, O. Jarjayes, T. J. Dunn, H. Vezin, M. Sakaguchi, T. Ogura, M. Orio, Y. Shimazaki, F. Thomas and T. Storr, *Chem. Eur. J.*, 2012, **18**, 14117-14127; (b) T. Storr, P. Verma, R. C. Pratt, E. C. Wasinger, Y. Shimazaki and T. D. P. Stack, *J. Am. Chem. Soc.*, 2008, **130**, 15448-15459; (c) L. Chiang, K. Herasymchuk, F. Thomas and T. Storr, *Inorg. Chem.*, 2015, **54**, 5970-5980; (d) T. Storr, E. C. Wasinger, R. C. Pratt and T. D. P. Stack, *Angew. Chem. Int. Ed.*, 2007, **46**, 5198-5201; (e) O. Rotthaus, O. Jarjayes, F. Thomas, C. Philouze, C. P. Del Valle, E. Saint-Aman and J. L. Pierre, *Chem. Eur. J.*, 2006, **12**, 2293-2302; (f) O. Rotthaus, F. Thomas, O. Jarjayes, C. Philouze, E. Saint-Aman and J. L. Pierre, *Chem. Eur. J.*, 2006, **12**, 6953-6962; (g) Y. Shimazaki, T. D. P. Stack and T. Storr, *Inorg. Chem.*, 2009, **48**, 8383-8392; (h) T. Kurahashi and H. Fujii, *J. Am. Chem. Soc.*, 2011, **133**, 8307-8316; (i) Y. Shimazaki, N. Arai, T. J.

Dunn, T. Yajima, F. Tani, C. F. Ramogida and T. Storr, *Dalton Trans.*, 2011, **40**, 2469-2479; (j) A. Kochem, O. Jarjayes, B. Baptiste, C. Philouze, H. Vezin, K. Tsukidate, F. Tani, M. Orio, Y. Shimazaki and F. Thomas, *Chem. Eur. J.*, 2012, **18**, 1068-1072; (k) P. Verma, R. C. Pratt, T. Storr, E. C. Wasinger and T. D. P. Stack, *Proc. Natl. Acad. Sci. U. S. A.*, 2011, **108**, 18600-18605; (l) D. de Bellefeuille, M. S. Askari, B. Lassalle-Kaiser, Y. Journaux, A. Aukauloo, M. Orio, F. Thomas and X. Ottenwaelder, *Inorg. Chem.*, 2012, **51**, 12796-12804; (m) K. Asami, K. Tsukidate, S. Iwatsuki, F. Tani, S. Karasawa, L. Chiang, T. Storr, F. Thomas and Y. Shimazaki, *Inorg. Chem.*, 2012, **51**, 12450-12461; (n) R. C. Pratt, C. T. Lyons, E. C. Wasinger and T. D. P. Stack, *J. Am. Chem. Soc.*, 2012, **134**, 7367-7377; (o) L. Lecarme, L. Chiang, C. Philouze, O. Jarjayes, T. Storr and F. Thomas, *Eur. J. Inorg. Chem.*, 2014, **2014**, 3479-3487; (p) M. Orio, O. Jarjayes, H. Kanso, C. Philouze, F. Neese and F. Thomas, *Angew. Chem. Int. Ed.*, 2010, **49**, 4989-4992; (q) Y. Shimazaki, F. Tani, K. Fukui, Y. Naruta and O. Yamauchi, *J. Am. Chem. Soc.*, 2003, **125**, 10512-10513.

19. O. Rotthaus, O. Jarjayes, C. P. Del Valle, C. Philouze and F. Thomas, *Chem. Commun.*, 2007, 4462-4464.

20. (a) K. Asami, A. Takashina, M. Kobayashi, S. Iwatsuki, T. Yajima, A. Kochem, M. van Gastel, F. Tani, T. Kohzuma, F. Thomas and Y. Shimazaki, *Dalton Trans.*, 2014, **43**, 2283-2293; (b) F. Thomas, O. Jarjayes, C. Duboc, C. Philouze, E. Saint-Aman and J.-L. Pierre, *Dalton Trans.*, 2004, 2662-2669; (c) M. P. Weberski Jr, C. C. McLauchlan and C. G. Hamaker, *Polyhedron*, 2006, **25**, 119-123; (d) M. E. Germain, T. R. Vargo, P. G. Khalifah and M. J. Knapp, *Inorg. Chem.*, 2007, **46**, 4422-4429.

21. (a) S. Y. Liu, J. D. Soper, J. Y. Yang, E. V. Rybak-Akimova and D. G. Nocera, *Inorg. Chem.*, 2006, **45**, 7572-7574; (b) S. Y. Liu and D. G. Nocera, *Tetrahedron Lett.*, 2006, **47**, 1923-1926; (c) D. J. Darensbourg, R. M. Mackiewicz, J. L. Rodgers, C. C. Fang, D. R. Billodeaux and J. H. Reibenspies, *Inorg. Chem.*, 2004, **43**, 6024-6034.

22. C. Bejger, Y. H. Tian, B. J. Barker, K. S. Boland, B. L. Scott, E. R. Batista, S. A. Kozimor and J. L. Sessler, *Dalton Trans.*, 2013, **42**, 6716-6719.

23. (a) N. G. Connelly and W. E. Geiger, *Chem. Rev.*, 1996, **96**, 877-910; (b) E. Steckhan, *Top. Curr. Chem.*, 1987, **142**, 1-69.

24. (a) A. Bjorn, *A Mechanistic Investigation of the Photochemical and Thermal Activation of 2,2- and 2,3-Diaryl and 2,2,3-Triaryl-2,3-dihydro-phenanthro[9,10-b]-1,4-dioxins, a New Class of 1,4-Dioxene Based DNA Cleaving Agents*, University of Cincinnati, 2002; (b) Y. Murata, F. Cheng, T. Kitagawa and K. Komatsu, *J. Am. Chem. Soc.*, 2004, **126**, 8874-8875; (c) T. J. Dunn, L. Chiang, C. F. Ramogida, K. Hazin, M. I. Webb, M. J. Katz and T. Storr, *Chem. Eur. J.*, 2013, **19**, 9606-9618.

25. R. C. Pratt and T. D. P. Stack, *Inorg. Chem.*, 2005, **44**, 2367-2375.

26. I. Noviandri, K. N. Brown, D. S. Fleming, P. T. Gulyas, P. A. Lay, A. F. Masters and L. Phillips, *J. Phys. Chem. B*, 1999, **103**, 6713-6722.

27. C. B. Hubschle, G. M. Sheldrick and B. Dittrich, *J. Appl. Crystallogr.*, 2011, **44**, 1281-1284.

28. O. V. Dolomanov, L. J. Bourhis, R. J. Gildea, J. A. K. Howard and H. Puschmann, *J. Appl. Crystallogr.*, 2009, **42**, 339-341.

29. G. M. Sheldrick, *Acta Crystallogr. A*, 2015, **71**, 3-8.

30. G. M. Sheldrick, *Acta Crystallogr. A*, 2008, **64**, 112-122.

31. P. van der Sluis and A. L. Spek, *Acta Crystallogr. A*, 1990, **46**, 194-201.

32. M. J. Frisch, G. W. Trucks, H. B. Schlegel, G. E. Scuseria, M. A. Robb, J. R. Cheeseman, G. Scalmani, V. Barone, B. Mennucci, G. A. Petersson, H. Nakatsuji, M. Caricato, X. Li, H. P. Hratchian, A. F. Izmaylov, J. Bloino, G. Zheng, J. L. Sonnenberg, M. Hada, M. Ehara, K. Toyota, R. Fukuda, J. Hasegawa, M. Ishida, T. Nakajima, Y. Honda, O. Kitao, H. Nakai, T. Vreven, J. Montgomery, J. A. , J. E. Peralta, F. Ogliaro, M. Bearpark, J. J. Heyd, E. Brothers, K. N. Kudin, V. N. Staroverov, R. Kobayashi, J. Normand, K. Raghavachari, A. Rendell, J. C. Burant, S. S. Iyengar, J. Tomasi, M. Cossi, N. Rega, N. J. Millam, M. Klene, J. E. Knox, J. B. Cross, V. Bakken, C. Adamo, J. Jaramillo, R. Gomperts, R. E. Stratmann, O. Yazyev, A. J. Austin, R. Cammi, C. Pomelli, J. W. Ochterski, R. L. Martin, K. Morokuma, V. G. Zakrzewski, G. A. Voth, P. Salvador, J. J. Dannenberg, S. Dapprich, A. D. Daniels, Ö. Farkas, J. B. Foresman, J. V. Ortiz, J. Cioslowski and D. J. Fox, *Gaussian 09, Revision A.02*, Gaussian, Inc., Wallingford, CT, 2009.

33. (a) A. D. Becke, *J. Chem. Phys.*, 1993, **98**, 5648-5652; (b) P. J. Stephens, F. J. Devlin, C. F. Chabalowski and M. J. Frisch, *J. Phys. Chem.*, 1994, **98**, 11623-11627.

34. (a) P. Fuentealba, H. Preuss, H. Stoll and L. Vonszentpaly, *Chem. Phys. Lett.*, 1982, **89**, 418-422; (b) A. Nicklass, M. Dolg, H. Stoll and H. Preuss, *J. Chem. Phys.*, 1995, **102**, 8942-8952.

35. (a) S. Miertus, E. Scrocco and J. Tomasi, *Chem. Phys.*, 1981, **55**, 117-129; (b) V. Barone, M. Cossi and J. Tomasi, *J. Comput. Chem.*, 1998, **19**, 404-417; (c) J. Tomasi, B. Mennucci and E. Cances, *J. Mol. Struct.*, 1999, **464**, 211-226; (d) V. Barone, M. Cossi and J. Tomasi, *J. Chem. Phys.*, 1997, **107**, 3210-3221.

36. (a) L. Castro, A. Yahia and L. Maron, *Dalton Trans.*, 2010, **39**, 6682-6692; (b) G. Li Manni, J. R. Walensky, S. J. Kraft, W. P. Forrest, L. M. Perez, M. B. Hall, L. Gagliardi and S. C. Bart, *Inorg. Chem.*, 2012, **51**, 2058-2064.

37. (a) M. E. Casida, in *In Recent Advances in Density Functional Methods*, ed. D. P. Chong, World Scientific, Singapore, 1995, p. 155; (b) R. E. Stratmann, G. E. Scuseria and M. J. Frisch, *J. Chem. Phys.*, 1998, **109**, 8218-8224.

38. A. D. Becke, *The Journal of Chemical Physics*, 1993, **98**, 1372-1377.

39. (a) A. Schafer, C. Huber and R. Ahlrichs, *J. Chem. Phys.*, 1994, **100**, 5829-5835; (b) A. Schafer, H. Horn and R. Ahlrichs, *J. Chem. Phys.*, 1992, **97**, 2571-2577.

40. (a) H. C. Hardwick, D. S. Royal, M. Helliwell, S. J. Pope, L. Ashton, R. Goodacre and C. A. Sharrad, *Dalton Trans.*, 2011, **40**, 5939-5952; (b) L. Cattalini, S. Degetto, M. Vidali and P. A. Vigato, *Inorg. Chim. Acta*, 1972, **6**, 173-176; (c) C. J. Burns, D. L. Clark, R. J. Donohoe, P. B. Duval, B. L. Scott and C. D. Tait, *Inorg. Chem.*, 2000, **39**, 5464-5468.

41. (a) M. Azam, S. I. Al-Resayes, G. Velmurugan, P. Venuvanalingam, J. Wagler and E. Kroke, *Dalton Trans.*, 2015, **44**, 568-577; (b) A. E. Vaughn, D. B. Bassil, C. L. Barnes, S. A. Tucker and P. B. Duval, *J. Am. Chem. Soc.*, 2006, **128**, 10656-10657; (c) G. Brancatelli, A. Pappalardo, G. Trusso Sfrazzetto, A. Notti and S. Geremia, *Inorg. Chim. Acta*, 2013, **396**, 25-29.

42. G. Bandoli, D. A. Clemente, U. Croatto, M. Vidali and P. A. Vigato, *Inorg. Nucl. Chem. Lett.*, 1972, **8**, 961-964.

43. (a) J. J. Katz, Seaborg, G.T., Morss, L.R., *The Chemistry of Actinide Elements*, Chapman and Hall, London, 1986; (b) M. S. Bharara, K. Strawbridge, J. Z. Vilsek, T. H. Bray and A. E. Gorden, *Inorg. Chem.*, 2007, **46**, 8309-8315; (c) C. Camp, L. Chatelain, V. Mougel, J. Pecaut and M. Mazzanti, *Inorg. Chem.*, 2015, **54**, 5774-5783.

44. J. B. Love, *Chem. Commun.*, 2009, 3154-3165.

45. D. L. Clark, S. D. Conradson, R. J. Donohoe, D. W. Keogh, D. E. Morris, P. D. Palmer, R. D. Rogers and C. D. Tait, *Inorg. Chem.*, 1999, **38**, 1456-1466.

46. M. J. Sarsfield and M. Helliwell, *J. Am. Chem. Soc.*, 2004, **126**, 1036-1037.

47. P. L. Arnold, D. Patel, A. J. Blake, C. Wilson and J. B. Love, *J. Am. Chem. Soc.*, 2006, **128**, 9610-9611.

48. (a) M. Sahin, A. Koca, N. Ozdemir, M. Dincer, O. Buyukgungor, T. Bal-Demirci and B. Ulkuseven, *Dalton Trans.*, 2010, **39**, 10228-10237; (b) R. D. Rogers, L. K. Kurihara and M. M. Benning, *J. Inclusion Phenom.*, 1987, **5**, 645-658; (c) L. Deshayes, N. Keller, M. Lance, M. Nierlich and J. D. Vigner, *Acta Crystallogr. C*, 1994, **50**, 1541-1544; (d) B. A. Maynard, J. C. Brooks, E. E. Hardy, C. J. Easley and A. E. Gorden, *Dalton Trans.*, 2015, **44**, 4428-4430.
49. L. Chiang, L. E. Allan, J. Alcantara, M. C. Wang, T. Storr and M. P. Shaver, *Dalton Trans.*, 2014, **43**, 4295-4304.
50. P. J. Melfi, S. K. Kim, J. T. Lee, F. Bolze, D. Seidel, V. M. Lynch, J. M. Veauthier, A. J. Gaunt, M. P. Neu, Z. Ou, K. M. Kadish, S. Fukuzumi, K. Ohkubo and J. L. Sessler, *Inorg. Chem.*, 2007, **46**, 5143-5145.
51. (a) M. S. Bharara, K. Heflin, S. Tonks, K. L. Strawbridge and A. E. Gorden, *Dalton Trans.*, 2008, 2966-2973; (b) A. A. Abu-Hussen and W. Linert, *Spectrochim. Acta A Mol. Biomol. Spectrosc.*, 2009, **74**, 214-223; (c) C. D. Sheela, C. Anitha, P. Tharmaraj and D. Kodimunthri, *J. Coord. Chem.*, 2010, **63**, 884-893.
52. (a) D. M. D'Alessandro and F. R. Keene, *Chem. Soc. Rev.*, 2006, **35**, 424-440; (b) M. B. Robin and P. Day, *Adv. Inorg. Chem. Radiochem.*, 1968, **10**, 247.
53. J. W. M. deBoer, Chen, K. S., Chung, Y. C. Chan, Wan, J. K. S., *J. Am. Chem. Soc.*, 1979, **101**, 3.
54. R. M. Clarke, K. Hazin, J. R. Thompson, D. Savard, K. E. Prosser and T. Storr, *Inorg. Chem.*, 2016, **55**, 762-774.
55. R. E. Stratmann, G. E. Scuseria and M. J. Frisch, *J. Chem. Phys.*, 1998, **109**, 8218-8224.
56. (a) R. L. Martin, *J. Chem. Phys.*, 2003, **118**, 4775-4777; (b) M. Mitoraj and A. Michalak, *J. Mol. Model.*, 2007, **13**, 347-355.